The gene for paroxysmal non-kinesigenic dyskinesia encodes an enzyme in a stress response pathway

Hsien-Yang Lee[1,2], Ying Xu[1], Yong Huang[1], Andrew H. Ahn[1], Georg W.J. Auburger[3],
Massimo Pandolfo[4], Hubert Kwieciński[5], David A. Grimes[6], Anthony E. Lang[7],
Jorgen E. Nielsen[8], Yuri Averyanov[9], Serenella Servidei[10], Andrzej Friedman[5],
Patrick Van Bogaert[4], Marc J. Abramowicz[4], Michiko K. Bruno[1,11], Beatrice F. Sorensen[1],
Ling Tang[2], Ying-Hui Fu[1] and Louis J. Ptáček[1,12],*

[1]Department of Neurology, UCSF, San Francisco, CA, USA, [2]Department of Human Genetics, University of Utah, Salt Lake City, UT, USA, [3]JW Goethe University Hospital, Frankfurt/M, Germany, [4]Erasme Hospital, Brussels, Belgium, [5]Department of Neurology, Medical Academy of Warsaw, Warsaw, Poland, [6]University of Ottawa, Ottawa Hospital, Division of Neurology, D715, Ottawa, Canada, [7]University of Toronto, Toronto Western Hospital, Toronto, Ontario, Canada, [8]Institute of Medical Biochemistry and Genetics, The Panum Institute, University of Copenhagen, Copenhagen, Denmark, [9]Clinic of Nervous Diseases, Moscow Medical Academy, Moscow, Russia, [10]Institute of Neurology, Catholic University, Rome, Italy, [11]National Institutes of Health/National Institute of Neurological Diseases and Stroke, Bethesda, MD, USA and [12]Howard Hughes Medical Institute, San Francisco, USA

Paroxysmal non-kinesigenic dyskinesia (PNKD) is characterized by spontaneous hyperkinetic attacks that are precipitated by alcohol, coffee, stress and fatigue. We report mutations in the myofibrillogenesis regulator 1 (*MR-1*) gene causing PNKD in 50 individuals from eight families. The mutations cause changes (Ala to Val) in the N-terminal region of two MR-1 isoforms. The MR-1L isoform is specifically expressed in brain and is localized to the cell membrane while the MR-1S isoform is ubiquitously expressed and shows diffuse cytoplasmic and nuclear localization. Bioinformatic analysis reveals that the *MR-1* gene is homologous to the hydroxyacylglutathione hydrolase (*HAGH*) gene. HAGH functions in a pathway to detoxify methylglyoxal, a compound present in coffee and alcoholic beverages and produced as a by-product of oxidative stress. Our results suggest a mechanism whereby alcohol, coffee and stress may act as precipitants of attacks in PNKD. Stress response pathways will be important areas for elucidation of episodic disease genetics where stress is a common precipitant of many common disorders like epilepsy, migraine and cardiac arrhythmias.

INTRODUCTION

Episodic neurologic diseases include rare mendelian phenotypes like the periodic paralyses, episodic ataxias and paroxysmal dyskinesias. Beginning with periodic paralysis, the causative genes have now been identified for many such disorders. Many of these encode homologous ion channels and led to definition of these disorders as the 'channelopathies'

(1–3). The familial paroxysmal dyskinesias (FPDs) are a group of hyperkinetic movement disorders; it has been hypothesized that mutations in ion channel genes may also be responsible for these disorders. We mapped the loci for 2 FPDs (4–6) but have not been able to identify mutations in candidate ion channel genes that were mapped to these loci.

Paroxysmal non-kinesigenic dyskinesia (PNKD) is an FPD characterized by intermittent attacks with any combination of
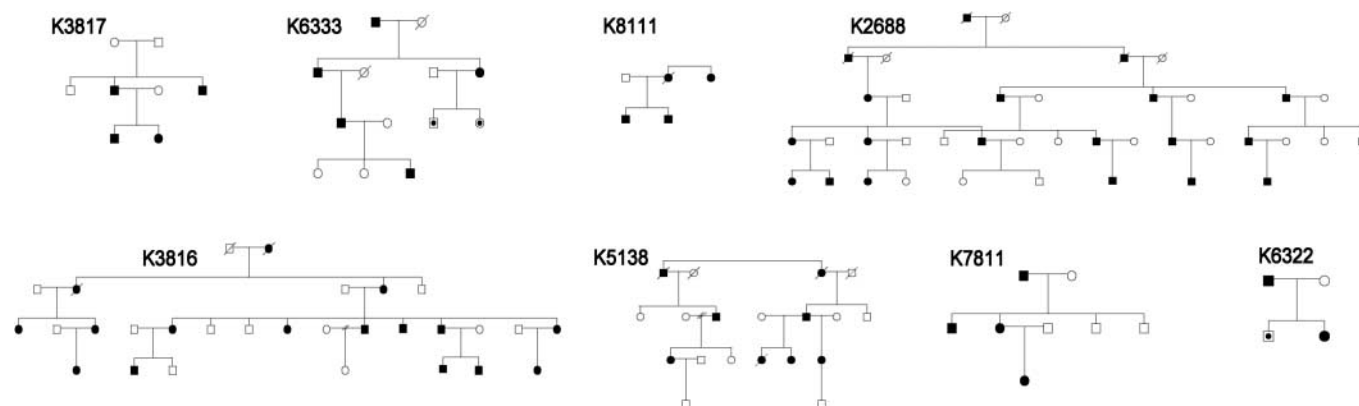
Figure 1. PNKD pedigrees. The A7V and A9V alleles segregate with the disease phenotype in all affected subjects. Five kindreds (K2688, K3816, K5138, K3817 and K8111) have the A7V mutation and three (K6333, K6322 and K7811) have the A9V mutation. Two asymptomatic gene carriers were identified; both were too young at the time of evaluation to be considered unaffected and are not included here. Circles are females; squares are males; filled circles and squares represent affected individuals; empty circles and squares denote unaffected individuals; a filled dot inside open circles or squares indicates that the individual's phenotype was uncertain.

dystonia, chorea, athetosis or ballismus (4,7–9). PNKD is an autosomal dominant disorder with high penetrance and can be precipitated by stress, fatigue, coffee, alcohol and menstruation (4,10). Age of onset is variable, but most commonly attacks start during childhood. PNKD attacks typically last from 10 min to 4 h and attack frequency can range from a few per year to several per day. PNKD attacks do not respond to antiepileptics, but benzodiazepines, such as Clonazepam, may be effective in alleviating the symptoms.

In addition to PNKD, paroxysmal dyskinesias include paroxysmal kinesigenic dyskinesia (PKD, attacks triggered by sudden voluntary movements), paroxysmal exercise-induced dyskinesia (PED, attacks are induced after prolonged exercise) and paroxysmal hypnogenic dyskinesia (PHD, attacks occur in sleep) (11). Most PHD cases are now thought to represent autosomal dominant nocturnal frontal lobe epilepsy, caused by mutations in nicotinic acetylcholine receptor genes (12–15). PKD is linked to the pericentromeric region of chromosome16 near the locus of infantile convulsions with choreoathetosis (ICCA syndrome) (5,6,16–18). Patients with paroxysmal choreoathetosis/spasticity (CSE) have dystonic posturing similar to that seen in PNKD patients, but physical exercise is a precipitating factor for triggering CSE. The gene for CSE has been localized to chromosome 1p between D1S443 and D1S197 but has not been identified (19).

PNKD was first mapped to a 10 Mb region on the long arm of chromosome 2 (4) and the region was subsequently narrowed to 4 Mb (20–22). We now report fine and physical mapping of the FPD1 locus to a ~3.0 Mb region and mutation analysis of the approximately 70 candidate genes in the region including a novel predicted gene myofibrillogenesis regulator 1 (*MR-1*). Sequencing of this gene revealed two distinct mutations in eight PNKD probands. Independently, another group has identified MR-1 mutations in two families (23). Although novel, MR-1 shares homology with the family of glyoxylases which function in the glutathione dependent metabolic pathway. Studies of the biology of MR-1 are likely to give new insights into the molecular pathogenesis of episodic

neurological phenomena and a possible rationale for 'stress' as a potent precipitant of episodic disorders.

RESULTS

Human subjects

Eighty-eight individuals (50 affected) from eight families were evaluated (Fig. 1). Age of attack onset was during infancy or early childhood in most patients, but there were three patients in kindred K3816 with attack onset at age 12, 18 and 21, and one patient in kindred K6333 with attack onset at age 12. The frequency of attacks varied considerably, ranging from daily to only a few times a year, even for affected subjects within the same kindred. Attack duration was between a few minutes and 8 h, but most patients reported typical attacks to be from 10 min up to 1 h. Attacks were characterized by both chorea and dystonia, and were usually precipitated by emotional stress, alcohol, coffee, fever, menstruation, hunger and/or exercise. There were no dramatic differences in phenotype among these families.

Mapping of the PNKD locus and mutation identification

Available microsatellite markers across the PNKD locus were used for fine mapping and haplotyping of the four initial PNKD families and revealed new recombinations that narrowed the PNKD locus to ~3.0 Mb. We constructed a physical contig of 50 overlapping bacterial artificial chromosomes (BACs) across the PNKD locus.

The disease haplotype was defined for the first four PNKD families (K2688, K3816, K5138 and K6333). Kindreds 5138 and 3816 shared a haplotype for 43 markers across a 650 kb region between D2S1338 and D2S2250, demonstrating that they share a common founder (Supplementary Material, Fig. S1). No other haplotype sharing was noted among these families. Both dHPLC and direct sequencing were used for mutation detection and revealed changes in *MR-1* in all

eight of the probands. Five of them had a change in the second position of the seventh codon causing an alanine to valine substitution (A7V). Three had a C to T transition in the second position of codon 9 causing an alanine to valine substitution (A9V). Both mutations are located in the N-terminal region of the *MR-1*L and *MR-1*S and are not present in *MR-1*M (discussed subsequently). They segregated with the disease allele in all of the eight PNKD families and were not present in over 250 unrelated controls. Exons from all three transcripts were examined and no other patient specific mutations were detected.

Multiple *MR-1* isoforms exist

Comparison of available genomic information in the databases (NCBI Human Genome, http://www.ncbi.nlm.nih.gov/genome/guide/human/; UCSC Genome Bioinformatics/Human Genome Browser Gateway, http://www.genome.ucsc.edu/cgi-bin/hgGateway; Ensembl Human Genome Browser, http://www.ensembl.org/Homo_sapiens) suggested that at least three alternatively spliced forms of *MR-1* exist consisting of 3, 9 and 10 exons. The genomic structures of these three forms of *MR-1* are shown in Figure 2A. Exons 1 and 2 are identical between *MR-1*L and *MR-1*S. Exons 3–10 of *MR-1*L are common to *MR-1*M. *MR-1*M has a unique 5′ exon encoding 56 amino acids. *MR-1*S has a unique 3′ exon that encodes 63 amino acids before a stop codon. The full length coding region of these three alternatively spliced forms have been PCR-amplified using human fetal brain cDNA as template and confirmed by direct sequencing (unpublished data). These unique exons encode protein sequences with no known homologies or motifs.

MR-1 is homologous to HAGH

Orthologs of *MR-1* were found in human, chimpanzee, mouse, rat, fugu and zebra fish, but not in *Caenorhabditis elegans*. By sequence similarity, hydroxyacylglutathione hydrolase (HAGH) was found to be most similar to MR-1L in the phylogenetic tree generated by genes homologous to *MR-1* (Supplementary Material, Fig. S2). These homologous proteins all contain β-lactamase domains characteristic of proteins encoded by genes in the metallo-β-lactamase superfamily. Biochemical analysis of the enzymatic functionality of MR-1 is in progress. The protein sequences encoded by the three exons of *MR-1*S and the unique exon of *MR-1*M are not homologous to any proteins in the database except vertebrate *MR-1* orthologs.

We generated a structural model of MR-1 using the 3D-Jigsaw software and verified homology between MR-1 and HAGH using the UCSF Chimera software (24,25). There was 41% identity between HAGH (260 residues) and MR-1L (385 residues) (107 identical, 50 conserved and 32 semi-conserved). All zinc binding residues (His54, His56, Asp58, His59, His110, Asp134 and His173) in HAGH (26) were found to be conserved in MR-1 (Supplementary Material, Fig. S3). Seven of the nine substrate binding residues (26) (Phe137, Cys141, His173, Tyr175, Asn179, Arg249 and Lys252) were conserved between human HAGH and MR-1, and the other two (K143R and Y145F) were conserved
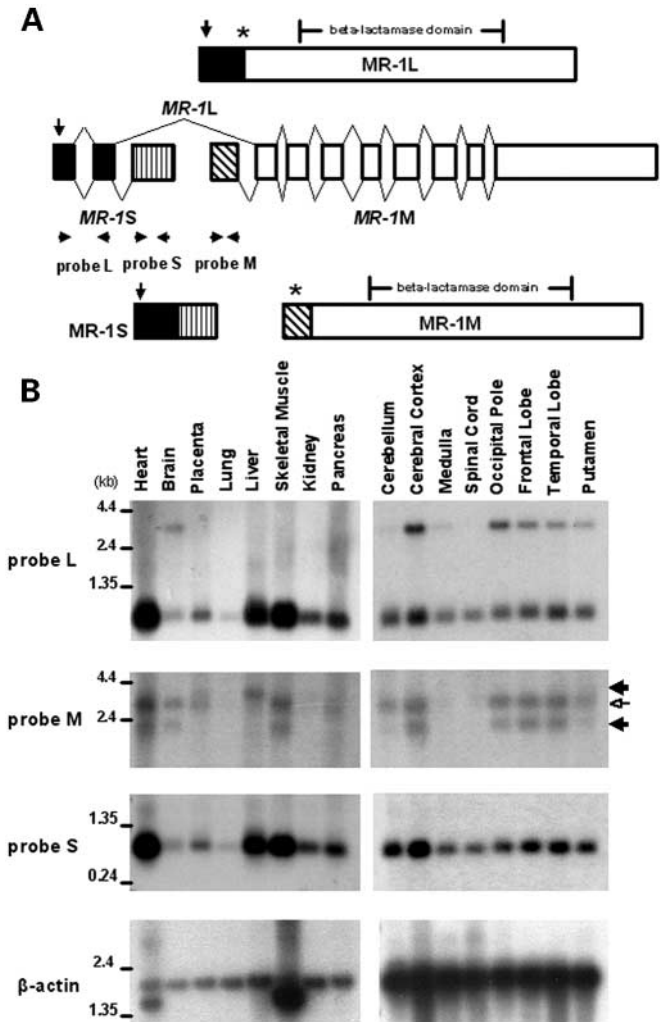
Figure 2. *MR-1* transcripts and isoforms. (**A**) The gene structure of three alternatively spliced forms of the *MR-1* gene is shown. Black rectangles represent exons shared by *MR-1*L and *MR-1*S; empty rectangles represent exons shared by *MR-1*L and *MR-1*M; the diagonal cross-hatched rectangle represents the unique exon of *MR-1*M; the rectangle with vertical hatches represents the unique exon of *MR-1*S. The vertical arrow marks the location of the A7V and A9V mutations. Horizontal arrows represent three probes for northern analysis: probe L for detecting *MR-1*L and *MR-1*S, probe M for detecting *MR-1*M and probe S for detecting *MR-1*S. The three predicted MR-1 isoforms are shown above and below the gene. The asterisks represent putative transmembrane domains of the MR-1L and MR-1M protein. (**B**) Northern blot analysis of *MR-1* (left, peripheral tissues; right, brain regions). The ~3 kb band (unfilled arrow) corresponds to the expected size of *MR-1*M. Two additional bands (~3.6 and ~2.0 kb) (**C**, filled arrows) are also seen. β-Actin was used as a loading control.

between yeast glyoxalases (GLO2 and GLO4) and MR-1. The two mutations are located in the N-terminal amino acid sequence which is present only in the L and S isoforms and is outside the β-lactamase domain.

Using the TMpred (27) program, a strong transmembrane region was predicted in MR-1M between residues 9 and 28. A weak transmembrane region was also predicted in MR-1L, between residues 74 and 92 (Fig. 2A and Supplementary Material, Fig. S4).

Northern analysis shows *MR-1*L is specifically expressed in brain

Three probes were generated to detect different splice forms (Fig. 2A). Probes L, M and S were designed to specifically detect *MR-1*L and S, *MR-1*M and *MR-1*S, respectively. Probe L detected two transcripts in both tissue and brain multiple tissue northern blots. The larger transcript was ∼3.2 kb and the smaller one was ∼0.8 kb, representing the L and S forms of *MR-1*, respectively. *MR-1*L was expressed exclusively and widely in the brain (Fig. 2B). Probe M of *MR-1* recognized at least three transcripts in different tissues and two transcripts in different brain regions ranging from ∼2 to >3 kb. The ∼3 kb band (Fig. 2B, unfilled arrow) corresponds to the expected size of *MR-1*M. Two additional bands (∼3.6 and ∼2.0 kb) (filled arrows) suggest that at least two additional transcripts exist. *MR-1*S is ubiquitously expressed in peripheral tissues and brain (Fig. 2B).

In situ hybridization of the *MR-1* ortholog in mouse CNS

Digoxygenin-labeled *BRP17* (the mouse ortholog of human *MR-1*) antisense riboprobe was used to detect mRNA expression in the mouse CNS. This riboprobe spans most of the coding region of the long *BRP17* transcript. Hydrolysed riboprobe was used as a 'universal' probe to detect the expression patterns of all *BRP17* transcripts in the mouse CNS.

In forebrain, *BRP17* was expressed in the cortex, hippocampus, dentate gyrus and medial and lateral habenula, and showed a strong expression pattern in several ventral regions, including the piriform cortex, amygdala and the ventromedial hypothalamic nucleus (Fig. 3A). The gene was also expressed in periaqueductal gray, *substantia nigra*, red nucleus, mammillary nucleus (Fig. 3B), raphe nucleus and interpeduncular nucleus (unpublished data). In cerebellum, *BRP17* was detected in both the granule cell and Purkinje cell layers, with strong reaction product in the granule cell layers of the lateral lobules and paraflocculus (Fig. 3C). Very little expression could be detected in the medulla (unpublished data). *BRP17* was exclusively expressed in a subset of neurons throughout the spinal cord, including all lamina of the dorsal horn and the motor neurons of the ventral horn (Fig. 3D).

Subcellular localization of MR-1

To investigate the subcellular localization of different isoforms of MR-1, we transfected wild-type MR-1−EGFP fusion protein constructs into HEK293 cells. The results showed that these three MR-1 isoforms have striking differences in their cellular distribution. MR-1S is found throughout the cytoplasm and in the nucleus (Fig. 4A). MR-1M is specifically localized in the perinuclear region (Fig. 4B). The CNS-specific MR-1L is localized mainly on the cell membrane (Fig. 4C and D). MR-1M co-localizes with a mitochondrial marker (Fig. 5). The different distribution of MR-1 isoforms suggests that they have distinct biological functions.

DISCUSSION

PNKD is an autosomal dominant paroxysmal dyskinesia manifested by attacks of chorea, dystonia and athetosis that can be precipitated by a variety of factors, including stress, hunger and fatigue (4,8,11,13). Other episodic neurological disorders sharing these precipitants and other clinical features with PNKD have been shown to result from ion channel gene mutations (reviewed in 1−3). We have previously ruled out ion channel genes as the cause of PNKD by extensive mutational analysis (unpublished data). Interestingly, coffee and alcohol are also potent precipitants of attacks in PNKD patients. Clonazepam is the best available treatment for this condition but is often ineffective in these patients. Thus, new targets for drug development may be important for this disorder and other episodic disesases.

Study of families with PNKD led to the genetic mapping of the disease allele and identification of *MR-1* as the PNKD gene. Independent patient-specific mutations occurring in conserved residues segregate with the phenotype in unrelated families, constituting strong genetic evidence that these mutations are causative. There were no recognizable differences in the clinical phenotypes of patients with the two different mutations or those reported elsewhere (23). PNKD is genetically homogeneous in our large collection of patients.

BRP17 is expressed in substantia nigra pars reticulata (SNR) and substantia nigra pars compacta (SNC), albeit at low levels (Fig. 3B). SNR and SNC are involved in the output and intrinsic modification of the basal ganglia activity, respectively (28−31). The basal ganglia plays a pivotal role in motor function (28,32). Dysfunction of the basal ganglia can result in either hypokinetic movement disorders (e.g. Parkinson's disease) or hyperkinetic movement disorders (e.g. Huntington's disease) (28,33,34).

BRP17 is also found in other regions involved in motor control, including the red nucleus and cerebral cortex (Fig. 3B), Purkinje and granule cells of the cerebellum (Fig. 3C) and the neurons located in the gray matter of the spinal cord (Fig. 3D). The high levels of expression in cortex and cerebellum are of particular interest in this phenotype. The expression of *MR-1/BRP17* in cerebellum, spinal cord and the basal ganglia, imply that *MR-1* plays an important role in maintaining excitability of these essential parts of the motor system. One caveat is that the *in situ* experiments reflect expression of three alternate transcripts including one (*MR-1M*) that does not contain the mutations.

MR-1 is homologous to HAGH (glyoxalase II), a member of the zinc metallohydrolase enzymes containing β-lactamase domains. The glyoxalase system consists of catalytic amounts of reduced glutathione and two enzymes, glyoxalase I and HAGH (glyoxalase II), and catalyses the conversion of methylglyoxal to D-lactate through the intermediate S-D-lactoylglutathione (Fig. 6) (35). The glyoxalase system is conserved through eukaryotic and prokaryotic species (35−38). Methylglyoxal has been shown to have mutagenic and carcinogenic activity (35,39) and it has also been found to have toxic effects on neuronal cells (40−42). Interestingly, though produced as a by-product of glycolysis, amino acid
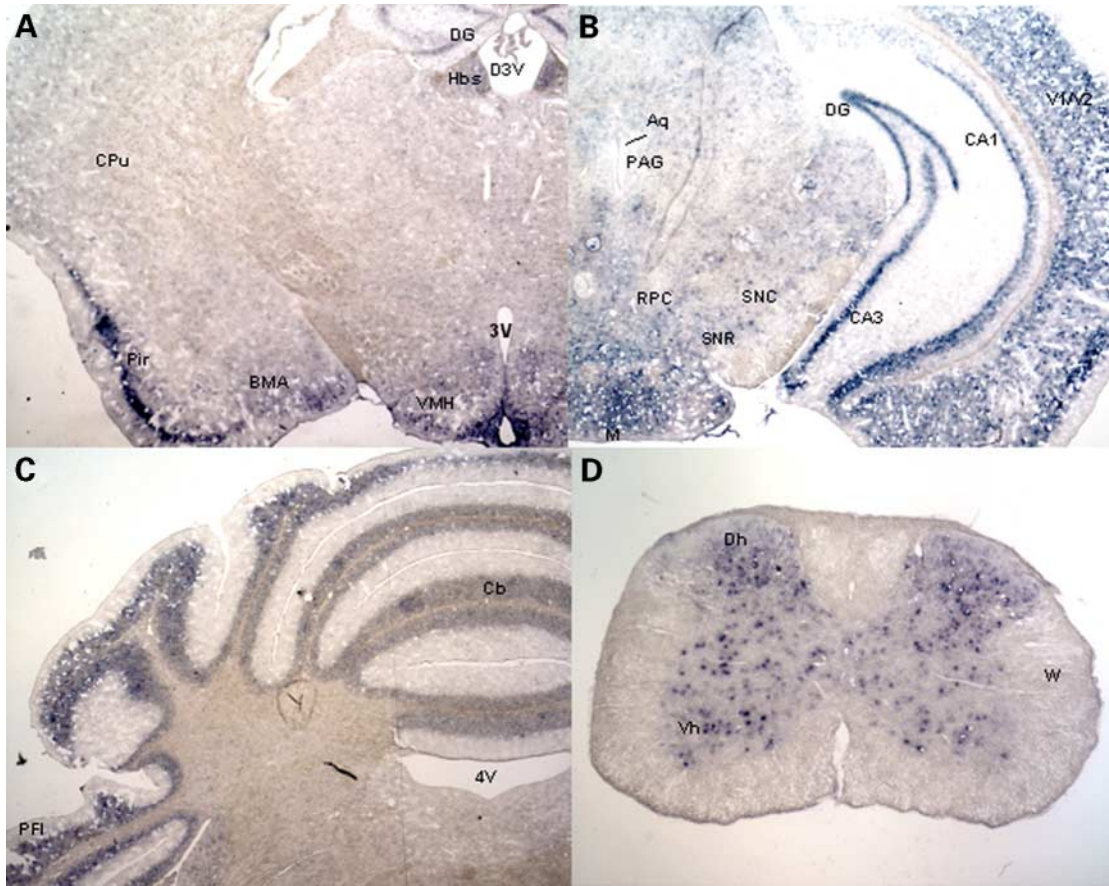
Figure 3. Localization of *BRP17* mRNA in mouse CNS by *in situ* hybridization. These 14 μm sections were hybridized with DIG-labeled antisense probe from the long form of *BRP17*. Representative sections from various regions are shown: (**A**) forebrain, (**B**) midbrain, (**C**) cerebellum, (**D**) spinal cord. Abbreviations used to label specific brain regions: DG, dentate gyrus; D3V, dorsal third ventricle; Hbs, medial and lateral habenula; 3V, third ventricle; Pir, piriform cortex; CPu, cautate putamen; BMA, basomedial amygdala; VMH, ventromedial thalamic nucleus; V1/V2, primary and secondary visual cortex; CA1 and CA3 fields of the hippocampus; Aq, aqueduct; PAG, periaqueductal gray; RPC, red nucleus; SNC, substantia nigra pars compacta; SNR, substantia nigra pars reticulata; M, mammilary nucleus; Cb, cerebellar lobule; 4V, fourth ventricle; PFl, paraflocculus; Dh, dorsal horn; Vh, ventral horn; W, white matter.
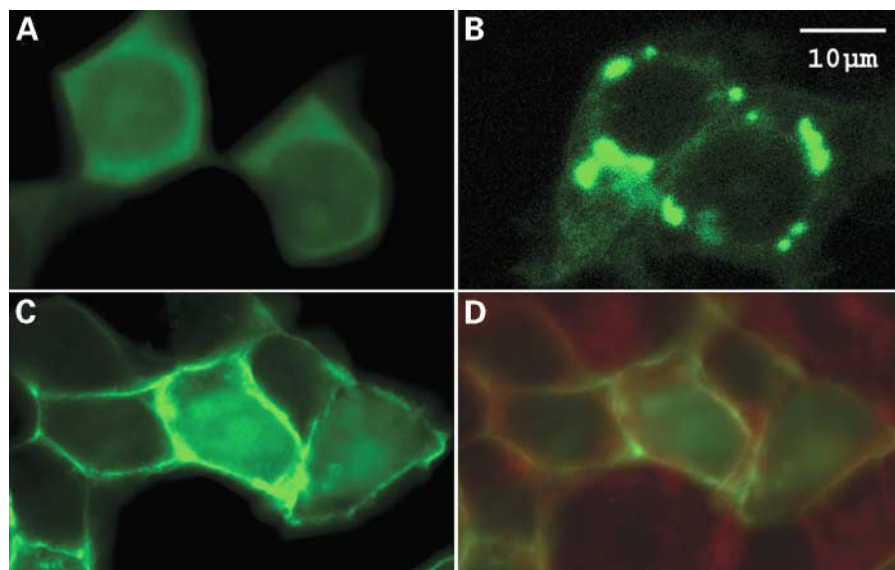
Figure 4. The localization patterns of MR-1 isoforms in HEK293 cells. (**A**) EGFP-tagged MR-1S showed a diffused pattern in cytoplasm and nucleus. (**B**) EGFP-tagged MR-1M presented a perinuclear pattern of localization. (**C**) EGFP-tagged MR-1L is located on the cell membrane. (**D**) The overlay image of the MR-1 long form (green) and the plasma membrane specific stain FM 4-64 (red) show co-localization in the plasma membrane.
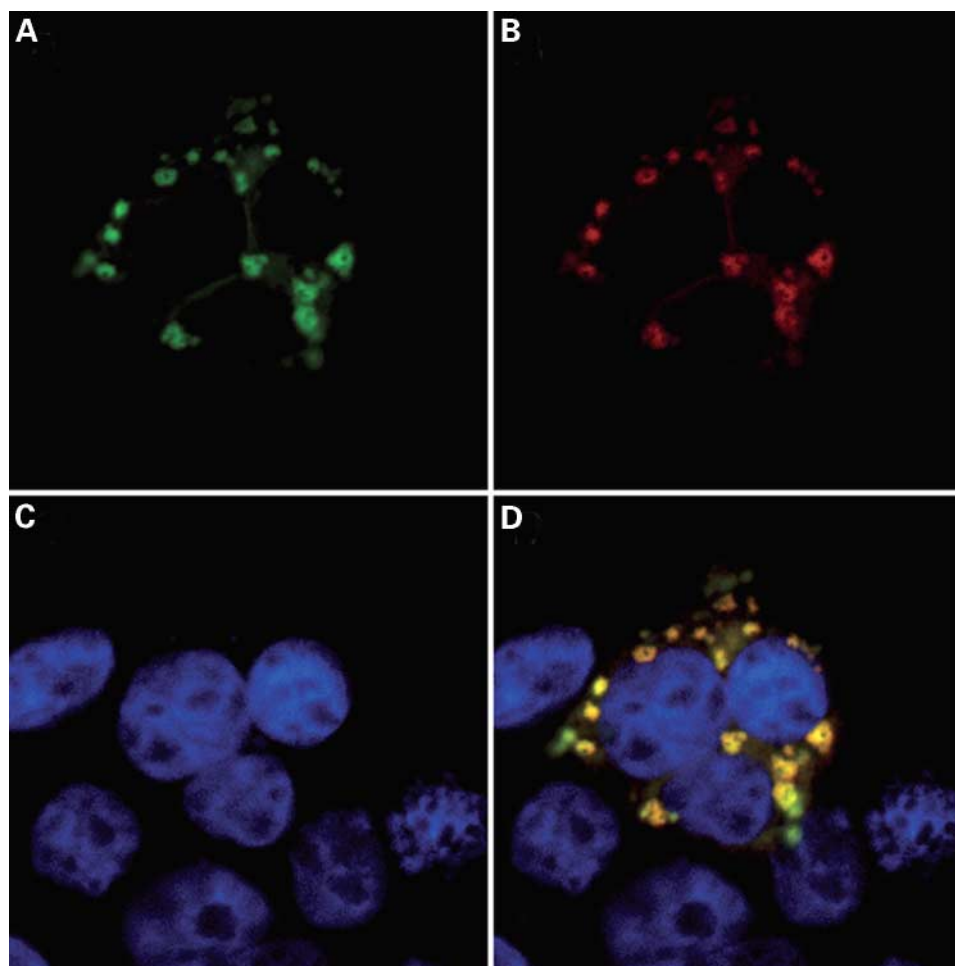
Figure 5. Localization of MR-1M in mitochondria. (**A**) EGFP-tagged MR-1M; (**B**) MitoTracker Red CMX Ros; (**C**) DAPI; (**D**) the merged image shows localization of MR-1M in mitochondria.
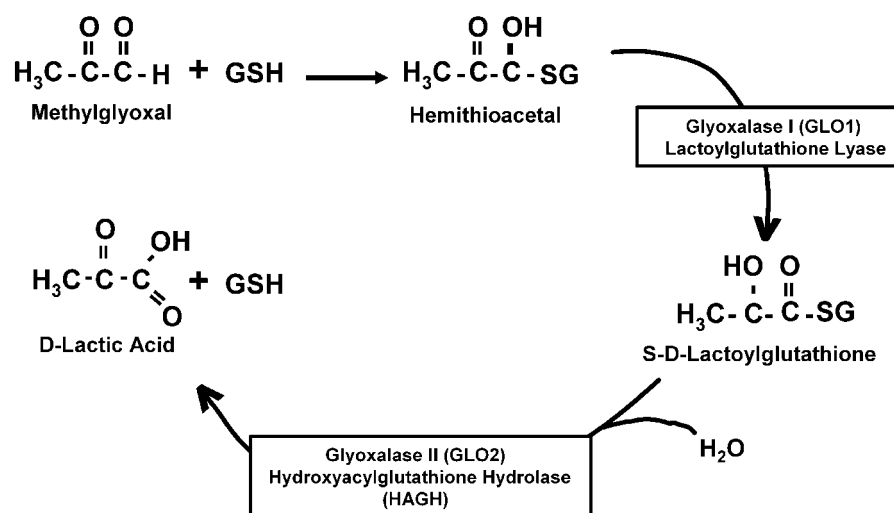
Figure 6. The glyoxylase system comprises two enzymes, glyoxylase I (GLO1, lactoylglutathione lyase) and glyoxylase II (GLOII, hydroxyacylglutathione hydrolase, HAGH). Methylglyoxal and glutathione non-enzymatically form a hemithioacetal intermediate and then glyoxylase I catalyzes formation of S-D-lactoylglutathione. HAGH catalyzes the hydrolysis of S-D-lactoylglutathione to D-lactate and reduced glutathione (GSH).

and ketone body metabolism (35,39), methylglyoxal is also found in considerable amounts in coffee, tea, cola and wine (43–45). HAGH has broad substrate specificity for glutathione thiol esters and hydrolyzes a number of these species to their corresponding carboxylic acids and reduced glutathione. Among these, 2-hydroxy thiol esters appear to be hydrolyzed with greatest efficiency (36). In mammalian cells, elevated methylglyoxal levels were observed during osmotic and oxidative stress.

The crystal structure of human HAGH has been solved and consists of two domains. The first domain folds into a four-layered β-sandwich, similar to that seen in the metallo-β-lactamases. The second domain is predominanatly α-helical. The active site contains a binuclear zinc-binding site and a substrate-binding site. MR-1L shows 41% identity to HAGH at the amino acid level and clusters closely with HAGH in the phylogenetic tree of glyoxalases (Supplementary Material, Fig. S2). All zinc binding residues are identical between these two proteins and seven out of the nine substrate binding residues are identical (Supplementary Material, Fig. S3). These results suggest that MR-1L is likely to have similar enzymatic activity to HAGH. Consistent with this hypothesis is the observation that PNKD attacks can be precipitated by alcohol and coffee, beverages known to contain high levels of methylglyoxal. However, additional work is necessary to determine with certainty the substrate(s) metabolized by MR-1 and the role of this biochemical pathway in neuronal excitability.

In addition to the region homologous to HAGH, MR-1L has a unique N-terminal region of 118 amino acids that does not show homology to any known protein. This N-terminal region of MR-1L (but not MR-1S) includes a potential transmembrane domain following a short peptide that may be a targeting signal for this protein and localization of its enzymatic function in neurons. This is consistent with our data showing localization of MR-1 in the membrane of cultured mammalian cells (Fig. 4). The PNKD mutations reside in the portion upstream of the transmembrane domain.

To our knowledge, all known glyoxalases are localized to cytoplasm or mitochondria. The neuron-specific, membrane-localization of MR-1L implies that this isoform has a unique biological function. Although the two MR-1 mutations we identified are not located in the β-lactamase domain, these mutations may cause dysfunction of the MR-1L via protein misfolding either by interfering with protein trafficking and/or localization or by interrupting normal interactions of MR-1 with other proteins.

Finally, though methylglyoxal is a toxin, there is data demonstrating that methylglyoxal modification of proteins as a consequence of increased reactive oxygen species can be a targeted process and that methylglyoxal may function as a signaling molecule in certain physiological processes (46). Furthermore, the product of the first step of this pathway, *S*-lactoylglutathione (Fig. 6), modulates assembly of microtubules *in vitro* and this has effects on certain cellular processes (47). Thus, one interesting possibility is that changes in the levels of methylglyoxal and/or *S*-lactoylglutathione as a result of MR-1 mutations may alter specific cell signaling processes in brain.

MATERIALS AND METHODS

Patient ascertainment

Subjects from eight families with PNKD were evaluated (Fig. 1). Written consent was obtained from all subjects in compliance with the Institutional Review Boards at the University of Utah Health Sciences Center and the University of California at San Francisco. Medical records of the affected members were reviewed and both the affected and unaffected members completed a questionnaire to confirm the presence and details of their movement disorders.

Physical mapping, fine mapping and construction of haplotypes

BACs were identified and isolated from the PCR-based human BAC library available from Research Genetics using known STSs in the PNKD locus. BAC end sequence was obtained using T7 and SP6 primers. These sequences were used to pull out additional overlapping BACs. This iterative process led to development of a BAC contig across the PNKD locus.

All known microsatellite markers were identified from the UCSC Genome Bioinformatics Human Genome Browser Gateway (http://www.genome.ucsc.edu/cgi-bin/hgGateway) and Ensembl Human Genome Browser (http://www.ensembl.org/Homo_sapiens). Primer sequences and information for the markers were obtained from the Genome Database (http://www.gdb.org). Screening of candidate genes revealed many additional polymorphisms in PNKD probands. These were genotyped in parents to set phase and combined with the results of microsatellite markers to define the disease haplotype in each family across the PNKD locus.

Mutational analysis

The genes located in the PNKD locus (between the centermetic border D2S173 and telomeric border D2S344) were screened for mutations by dHPLC and direct sequencing (including coding sequence and 5′- and 3′-UTRs of three alternatively spliced forms) of genomic DNA from the four initial PNKD probands. Fifty microliters of PCR reactions were performed with 100 ng of genomic DNA and 10 pmol of each forward and reverse primer. The primers were designed outside the splice sites so that intronic sequence of at least 50 bp flanking each exon boundary could be obtained. *MR-1* primers are shown in Supplementary Material, Table S1. PCR reactions were performed with the following protocol: 94°C, 3 min (94°C, 30 s; 60°C, 30 s; 72°C, 30 s) × 40, 72°C, 3 min and 15°C hold. The PCR products were purified using the PCR$_{96}$ Cleanup Plate (Millipore, Bedford, MA, USA) and were sequenced. For dHPLC mutation detection, 10 μl of the PCR products were analyzed by the WAVE nucleic acid fragment analysis system (Transgenomic, Omaha, NE, USA). The following primers were used for detection of the mutations: primer-F 5′-GCT TCT GGG AGA TGT AGT TTC TGG TC-3′ and primer-R 5′-CAA GAG CCC TGA CCT CCT GCT ATC-3′. The following primers were used for dHPLC detection of the mutations with an oven temperature of 67.3°C: primer-dF 5′-CCTGGG AAG AGT AGT TCT CCT G-3′ and primer-dR 5′-GCC CCC GCC CGC GGG GTC CCT CTC CTT AC-3′.

Bioinformatic analysis of *MR-1*

In order to find homologous genes, we aligned the MR-1 protein sequences against NCBI's non-redundant protein data-base using WU-BLAST (http://blast.wustl.edu). Sequences with BLAST expectation values less than 1×10^{-10} were used for multiple alignments. Multiple sequence alignment was done using the T-Coffee software (48). Another software package, Lobster, was used to cross-check the results from T-Coffee (49). Rebuilding the phylogenetic tree was done with ClustalW software (50). Most of these sequences contain β-lactamase domains, so multiple alignments were performed on both the full sequences and the sequence fragments corresponding to the β-lactamase domain predicted by PFAM (51).

Cloning of *MR-1* cDNAs

Three alternatively spliced full-length transcripts of *MR-1* (Fig. 2; long, medium and short are *MR-1*L, *MR-1*M and *MR-1*S, respectively) were PCR-amplified from human fetal brain cDNA. The primer sets used to clone these *MR-1* cDNAs were: primerL-F 5′-GAA GCG GGG GTG GGA TCT-3′, primerL-R 5′-CCT CAC AGT CTC ATC GCC TGA T-3′, primerM-F 5′-AGC ATG GCT TGG CAG GGC TG-3′, primerM-R 5′-GTG TTA GCG ATG AGA AGG ATG ATG-3′, primerS-F 5′-CGG GGG TGG GAT CTG AAC-3′, primerS-R 5′-CCT GAG GAC TTA ACA GTC AAT A-3′. These PCR products were purified and cloned into the TOPO TA cloning vector (Invitrogen, Carlsbad, CA, USA). These TA clones were then used as templates and PCR-amplified with primers containing *Xho*I and *Pst*I sites at 5′ and 3′ ends. The PCR products were then gel-purified with the QIAquick gel extraction kit (Qiagen, Valencia, CA, USA) and subcloned into the pGEM-T Easy vector system (Promega, Madison, WI, USA). The different forms of *MR-1* cloned into T Easy vectors were then digested by *Xho*I and *Pst*I, gel-purified and cloned into the *Xho*I–*Pst*I site of the pEGFP-N1 vector (Clontech, Palo Alto, CA, USA) by the LigaFast rapid DNA ligation system (Promega). Clones were sequenced to confirm that no new mutations had been introduced.

For *in situ* hybridization experiments, the long form of *BRP17* (mouse brain protein 17, the mouse *MR-1* ortholog) was PCR-amplified from mouse brain cDNA. The primers used for cloning *BRP17* were: primerBRP-F 5′-GCT GTT GGC TGC TAT TCT TCG-3′, primerBRP-R 5′-TTC TCA GGA ATG GGT TGT AGG C-3′. The PCR product was pur-ified and cloned into the TOPO TA cloning vector. After digestion with *Xho*I and *Spe*I, the *BRP17* gene was sub-cloned into the pBluescript II KS(+) vector (Stratagene, La Jolla, CA, USA).

Northern analysis

Commercial human multiple tissue northern blots (peripheral tissues and brain regions, Clontech) were hybridized with probes specific for each of the transcripts (nucleotides 46–235 of *MR-1*L, nucleotides 43–140 of *MR-1*M and nucleotides 237–474 of *MR-1*S, Fig. 2). Probes were generated by PCR of

human fetal brain cDNA using the following primers: probe LF 5′-AGA AAT GCC CGC GTC CTC-3′, probe LR 5′-AGG CCA GTC CCA CAG CTT TC-3′, probe MF 5′-GGC TGC TGG CTC CTC CTC-3′, probe MR 5′-CTG GCT GTG CGC CAT GAG-3′, probe SF 5′-TCC CTT GTG GTA TCC TCC TCT T-3′ and probe SR 5′-CCT GAG GAC TTA ACA GTC AAT AGC C-3′ and were labeled with [α-^{32}P]dCTP using the Rediprime II random prime labeling system (Amersham, Piscataway, NJ, USA). A β-actin probe was used as a loading control. Hybridization and wash were performed pursuant to the protocol provided by the manufac-turer. The blots were exposed to X-OMAT AR X-ray film (Kodak, Rochester, NY, USA) and placed on intensifying screens at −70°C for 36–72 h.

In situ hybridization

The subjects were adult male C57/BL6 mice weighing 30–50 g (Charles River, Pleasanton, CA, USA) and were con-ducted on protocols approved by the Institutional Animal Care and Use Committee in accordance with the NIH Guide for the Care and Use of Laboratory Animals (1996). The mice were sacrificed by lethal i.p. injection of sodium pento-barbital (150 mg/kg) and intracardially perfused with saline, followed by fixation with 4% formaldehyde in 0.1 M sodium phosphate (pH 7.4). Brains and spinal cords were removed and post-fixed in the same fixative for 4 h, then cryoprotected overnight in 30% sucrose in 0.1 M sodium phosphate (pH 7.4). Coronal sections were cut at 14 μm and thaw-mounted onto Superfrost Plus slides (Fisher, Pittsburgh, PA, USA).

To make an antisense riboprobe, a PCR product correspond-ing to nucleotides 44–958 of the long form *BRP17* gene was cloned into pBluescript II KS(+). Antisense digoxigenin (DIG)-labeled riboprobe was made with T7 RNA polymerase and the DIG RNA labeling kit (Roche Molecular Bio-chemicals, Indianapolis, IN, USA). The riboprobe was then hydrolysed to 100–300 bp fragments by alkaline hydrolysis at 60°C, and neutralized with glacial acetic acid and sodium acetate. Yeast tRNA (Ambion, Austin, TX, USA) was added as carrier, then precipitated and subsequently stored at −80°C.

Sections were pre-hybridized in the hybridization solution (50% deionized formamide, 10% dextran sulfate, 0.3 M NaCl, 0.02 M Tris, 5 mM EDTA, 0.01 M NaH$_2$PO$_4$, 1×Denhardt's, and 0.5 mg/ml yeast tRNA) at 60°C for 1 h in a humidified chamber. A dilution of DIG-labeled *BRP17* antisense riboprobe (1:75) was prepared (1 μl of probe per 50 μl hybridization sol-ution) and denatured at 85°C for 5 min followed by quenching on ice for 2 min. The slides were then placed in hybridization solution and incubated overnight at 60°C in a humidified chamber. The hybridization was ended by placing the slides in 4 × SSC at room temperature, then followed by four washes at 60°C, 15 min each in 4 × SSC, 4 × SSC/50% forma-mide and two sequential washes of 2 × SSC and 0.2 × SSC.

To detect digoxigenin label, room temperature (RT) washes were made using a DIG detection kit (Roche). After a wash in DIG wash buffer, the sections were incubated in block buffer for 1 h. Sections were then incubated with alkaline phospha-tase-linked anti-DIG antibody (Roche) at 1:1000 dilution in 1×block buffer at RT for 1 h. Sections were then washed in 1×DIG wash buffer three times for 10 min, incubated in

$1\times$ alkaline detection buffer for 5 min, and incubated overnight at 4°C with BM Purple with 0.1% Tween 20 (Roche) in a humidified chamber. Finally, the sections were rinsed in 10 mM Tris with 1 mM EDTA and then mounted under cover slides with Fluoromount G (Electron Microscopy Sciences, Washington, PA, USA). Images were captured with a Nikon Eclipse microscope with CCD camera and were imported into Photoshop (Adobe System, San Jose, CA, USA) for analysis.

Mammalian cell culture and transfection

Human embryonic kidney (HEK)-293 cells were grown in Dulbecco's modified Eagle's medium (DMEM) supplemented with penicillin, streptomycin and 10% fetal bovine serum (Hyclone, Logan, UT, USA) and maintained at 37°C with 5% CO_2. After 1 day, the cells were split into 35 mm culture dishes on coverslips pre-coated with poly-L-lysine (Sigma, St Louis, MO, USA). In parallel, HEK293 cells grown to 80–90% confluence were transfected with 2 µg DNA (pEGFP-N1 alone and the *MR-1*L, M and S wild-type fusion constructs) using 20 µl of Polyfect reagent (Qiagen) using a standard protocol. Twelve hours post-transfection, cell membrane staining was carried out by applying 5–10 µM of plasma membrane-specific dye FM 4–64 or 50 nM of mitochondria-specific probe MitoTracker Red CMXRos (Molecular Probes, Eugene, OR, USA) to culture medium followed by 15–30 min incubation. Cells were then fixed with 4% paraformaldehyde in phosphate buffer for 10 min, rinsed in PBS (pH 7.4) and mounted on Premium microscope slides (Fisher, Pittsburgh, PA, USA) with Vectashield mounting medium (Vector, Burlingame, CA, USA). Images were acquired using the Zeiss Pascal LSM5 confocal microscope in the UCSF microscopy core facility.

SUPPLEMENTARY MATERIAL

Supplementary Material is available at HMG Online.

ACKNOWLEDGEMENTS

REFERENCES

1. Jen, J. and Ptacek, L.J. (2001) Channelopathies. In Scriver, C.R., Beaudet, A.L., Sly, W.S. and Valle, D. (eds), *Metabolic and Molecular Bases of Inherited Disease*, 8th ed. McGraw-Hill, New York, pp. 5223–5238.
2. Lenz, R. and Ptacek, L.J. (2004) Channelopathies. In Bradley, W.G., Daroff, R.B., Fenichel, G. and Jankovic, J. (eds), *Neurology in Clinical Practice*, 4th ed. Butterworth-Heinemann, Philadelphia, pp. 1847–1866.
3. Ptacek, L.J. and Fu, Y.H. (2001) Channelopathies: episodic disorders of the nervous system. *Epilepsia*, **42**, 35–43.
4. Fouad, G.T., Servidei, S., Durcan, S., Bertini, E. and Ptacek, L.J. (1996) A gene for familial paroxysmal dyskinesia (FPD1) maps to chromosome 2q. *Am. J. Hum. Genet.*, **59**, 135–139.
5. Bennett, L.B., Roach, E.S. and Bowcock, A.M. (2000) A locus for paroxysmal kinesigenic dyskinesia maps to human chromosome 16. *Neurology*, **54**, 125-130.
6. Swoboda, K.J., Soong, B., McKenna, C., Brunt, E.R., Litt, M., Bale, J.F., Jr., Ashizawa, T., Bennett, L.B., Bowcock, A.M., Roach, E.S. et al. (2000) Paroxysmal kinesigenic dyskinesia and infantile convulsions: clinical and linkage studies. *Neurology*, **55**, 224–230.
7. Richards, R.N. and Barnett, H.J. (1968) Paroxysmal dystonic choreoathetosis. A family study and review of the literature. *Neurology*, **18**, 461–469.
8. Mount, L.A. and Reback, S. (1940) Familial paroxysmal choreoathetosis: preliminary report on a hithero undescribed clinical syndrome. *Arch. Neurol. Psychiatry*, **44**, 841–847.
9. Bressman, S.B., Fahn, S. and Burke, R.E. (1988) Paroxysmal non-kinesigenic dystonia. *Adv. Neurol.*, **50**, 403–413.
10. Matsuo, H., Kamakura, K., Saito, M., Okano, M., Nagase, T., Tadano, Y., Kaida, K., Hirata, A., Miyamoto, N., Masaki, T. et al. (1999) Familial paroxysmal dystonic choreoathetosis: clinical findings in a large Japanese family and genetic linkage to 2q. *Arch. Neurol.*, **56**, 721–726.
11. Demirkiran, M. and Jankovic, J. (1995) Paroxysmal dyskinesias: clinical features and classification. *Ann. Neurol.*, **38**, 571–579.
12. Steinlein, O.K., Mulley, J.C., Propping, P., Wallace, R.H., Phillips, H.A., Sutherland, G.R., Scheffer, I.E. and Berkovic, S.F. (1995) A missense mutation in the neuronal nicotinic acetylcholine receptor alpha 4 subunit is associated with autosomal dominant nocturnal frontal lobe epilepsy. *Nat. Genet.*, **11**, 201–203.
13. Ptacek, L.J. and Fu, Y.H. (2002) Molecular biology of episodic movement disorders. *Adv. Neurol.*, **89**, 453–458.
14. Phillips, H.A., Scheffer, I.E., Crossland, K.M., Bhatia, K.P., Fish, D.R., Marsden, C.D., Howell, S.J., Stephenson, J.B., Tolmie, J., Plazzi, G. et al. (1998) Autosomal dominant nocturnal frontal-lobe epilepsy: genetic heterogeneity and evidence for a second locus at 15q24. *Am. J. Hum. Genet.*, **63**, 1108–1116.
15. Gambardella, A., Annesi, G., De Fusco, M., Patrignani, A., Aguglia, U., Annesi, F., Pasqua, A.A., Spadafora, P., Oliveri, R.L., Valentino, P. et al. (2000) A new locus for autosomal dominant nocturnal frontal lobe epilepsy maps to chromosome 1. *Neurology*, **55**, 1467–1471.
16. Szepetowski, P., Rochette, J., Berquin, P., Piussan, C., Lathrop, G.M. and Monaco, A.P. (1997) Familial infantile convulsions and paroxysmal choreoathetosis: a new neurological syndrome linked to the pericentromeric region of human chromosome 16. *Am. J. Hum. Genet.*, **61**, 889–898.
17. Lee, W.L., Tay, A., Ong, H.T., Goh, L.M., Monaco, A.P. and Szepetowski, P. (1998) Association of infantile convulsions with paroxysmal dyskinesias (ICCA syndrome): confirmation of linkage to human chromosome 16p12–q12 in a Chinese family. *Hum. Genet.*, **103**, 608–612.
18. Tomita, H., Nagamitsu, S., Wakui, K., Fukushima, Y., Yamada, K., Sadamatsu, M., Masui, A., Konishi, T., Matsuishi, T., Aihara, M. et al. (1999) Paroxysmal kinesigenic choreoathetosis locus maps to chromosome 16p11.2–q12.1. *Am. J. Hum. Genet.*, **65**, 1688–1697.
19. Auburger, G., Ratzlaff, T., Lunkes, A., Nelles, H.W., Leube, B., Binkofski, F., Kugel, H., Heindel, W., Seitz, R., Benecke, R. et al. (1996) A gene for autosomal dominant paroxysmal choreoathetosis/spasticity (CSE) maps to the vicinity of a potassium channel gene cluster on chromosome 1p, probably within 2 cM between D1S443 and D1S197. *Genomics*, **31**, 90–94.
20. Hofele, K., Benecke, R. and Auburger, G. (1997) Gene locus FPD1 of the dystonic Mount-Reback type of autosomal-dominant paroxysmal choreoathetosis. *Neurology*, **49**, 1252–1257.
21. Fink, J.K., Hedera, P., Mathay, J.G. and Albin, R.L. (1997) Paroxysmal dystonic choreoathetosis linked to chromosome 2q: clinical analysis and proposed pathophysiology. *Neurology*, **49**, 177–183.
22. Raskind, W.H., Bolin, T., Wolff, J., Fink, J., Matsushita, M., Litt, M., Lipe, H. and Bird, T.D. (1998) Further localization of a gene for paroxysmal dystonic choreoathetosis to a 5-cM region on chromosome 2q34. *Hum. Genet.*, **102**, 93–97.
23. Rainier, S., Thomas, D., Tokarz, D., Ming, L., Bui, M., Plein, E., Zhao, X., Lemons, R., Albin, R., Delaney, C. et al. (2004) Myofibrillogenesis

regulator 1 gene mutations cause paroxysmal dystonic choreoathetosis. *Arch. Neurol.*, **61**, 1025–1029.

24. Bates, P.A., Kelley, L.A., MacCallum, R.M. and Sternberg, M.J. (2001) Enhancement of protein modeling by human intervention in applying the automatic programs 3D-JIGSAW and 3D-PSSM. *Proteins*, **5** (suppl.), 39–46

25. Huang, C.C., Couch, G.S., Pettersen, E.F. and Ferrin, T.E. (1996) Chimera: an extensible molecular modeling application constructed using standard components. *Pacific Symp. Biocomput.*, **1**, 724.

26. Cameron, A.D., Ridderstrom, M., Olin, B. and Mannervik, B. (1999) Crystal structure of human glyoxalase II and its complex with a glutathione thiolester substrate analogue. *Structure Fold Des.*, **7**, 1067–1078.

27. Hofmann, K. and Stoffel, W. (1993) TMbase—a database of membrane spanning proteins segments. *Biol. Chem. Hoppe-Seyler*, **374**, 166.

28. Mink, J.W. (2003) The basal ganglia and involuntary movements: impaired inhibition of competing motor patterns. *Arch. Neurol.*, **60**, 1365–1368.

29. Herrero, M.T., Barcia, C. and Navarro, J.M. (2002) Functional anatomy of thalamus and basal ganglia. *Child Nerv. Syst.*, **18**, 386–404.

30. Parent, A. and Hazrati, L.N. (1995) Functional anatomy of the basal ganglia. I. The cortico-basal ganglia-thalamo-cortical loop. *Brain Res. Brain Res. Rev.*, **20**, 91–127.

31. Parent, A. and Hazrati, L.N. (1995) Functional anatomy of the basal ganglia. II. The place of subthalamic nucleus and external pallidum in basal ganglia circuitry. *Brain Res. Brain Res. Rev.*, **20**, 128–154.

32. Trost, M. (2003) Dystonia update. *Curr. Opin. Neurol.*, **16**, 495–500.

33. Richter, A. and Loscher, W. (2002) Animal models of paroxysmal dystonia. *Adv. Neurol.*, **89**, 443–451.

34. Vitek, J.L. (2002) Pathophysiology of dystonia: a neuronal model. *Mov. Disord.*, **17**, S49–62.

35. Thornalley, P.J. (1993) The glyoxalase system in health and disease. *Mol. Aspects. Med.*, **14**, 287–371.

36. Ridderstrom, M., Saccucci, F., Hellman, U., Bergman, T., Principato, G. and Mannervik, B. (1996) Molecular cloning, heterologous expression, and characterization of human glyoxalase II. *J. Biol. Chem.*, **271**, 319–323.

37. Bito, A., Haider, M., Hadler, I. and Breitenbach, M. (1997) Identification and phenotypic analysis of two glyoxalase II encoding genes from *Saccharomyces cerevisiae*, *GLO2* and *GLO4*, and intracellular localization of the corresponding proteins. *J. Biol. Chem.*, **272**, 21509–21519.

38. Bito, A., Haider, M., Briza, P., Strasser, P. and Breitenbach, M. (1999) Heterologous expression, purification, and kinetic comparison of the cytoplasmic and mitochondrial glyoxalase II enzymes, Glo2p and Glo4p, from *Saccharomyces cerevisiae*. *Protein Expr. Purif.*, **17**, 456–464.

39. Thornalley, P.J. (1996) Pharmacology of methylglyoxal: formation, modification of proteins and nucleic acids, and enzymatic detoxification— a role in pathogenesis and antiproliferative chemotherapy. *Gen. Pharmacol.*, **27**, 565–573.

40. Davies, M.G., Chambers, P.L. and Rowan, M.J. (1986) Effects of Methylglyoxal on Central and Peripheral Cholinergic Responses. *Arch. Toxicol.*, **9** (suppl.), 46–50.

41. Kikuchi, S., Shinpo, K., Moriwaka, F., Makita, Z., Miyata, T. and Tashiro, K. (1999) Neurotoxicity of methylglyoxal and 3-deoxyglucosone on cultured cortical neurons: synergism between glycation and oxidative stress, possibly involved in neurodegenerative diseases. *J. Neurosci. Res.*, **57**, 280–289.

42. Shinpo, K., Kikuchi, S., Sasaki, H., Ogata, A., Moriwaka, F. and Tashiro, K. (2000) Selective vulnerability of spinal motor neurons to reactive dicarbonyl compounds, intermediate products of glycation, in vitro: implication of inefficient glutathione system in spinal motor neurons. *Brain Res.*, **861**, 151–159.

43. Hayashi, T. and Shibamoto, T. (1985) Analysis of methylglyoxal in foods and beverages. *J. Agric. Food Chem.*, **33**, 1090–1093.

44. Nagao, M., Fujita, Y., Sugimura, T. and Kosuge, T. (1986) Methylglyoxal in beverages and foods: its mutagenicity and carcinogenicity. *IARC Sci. Publ.*, **70**.

45. Nagao, M., Fujita, Y., Wakabayashi, K., Nukaya, H., Kosuge, T. and Sugimura, T. (1986) Mutagens in coffee and other beverages. *Environ. Health Perspect*, **67**, 89–91.

46. Van Herreweghe, F., Mao, J., Chaplen, F.W., Grooten, J., Gevaert, K., Vandekerckhove, J. and Vancompernolle, K. (2002) Tumor necrosis factor-induced modulation of glyoxalase I activities through phosphorylation by PKA results in cell death and is accompanied by the formation of a specific methylglyoxal-derived AGE. *Proc. Natl Acad. Sci. USA*, **99**, 949–954.

47. Gillespie, E. (1979) Effects of *S*-lactoylglutathione and inhibitors of glyoxalase I on histamine release from human leukocytes. *Nature*, **277**, 135–137.

48. Notredame, C., Higgins, D.G. and Heringa, J. (2000) T-Coffee: a novel method for fast and accurate multiple sequence alignment. *J. Mol. Biol.*, **302**, 205–217.

49. Edgar, R.C. and Sjolander, K. (2003) SATCHMO: sequence alignment and tree construction using hidden Markov models. *Bioinformatics*, **19**, 1404–1411.

50. Higgins, D.G., Bleasby, A.J. and Fuchs, R. (1992) CLUSTAL V: improved software for multiple sequence alignment. *Comput. Appl. Biosci.*, **8**, 189–191.

51. Bateman, A., Coin, L., Durbin, R., Finn, R.D., Hollich, V., Griffiths-Jones, S., Khanna, A., Marshall, M., Moxon, S., Sonnhammer, E.L. *et al.* (2004) The Pfam protein families database. *Nucl. Acids Res.*, **32**, D138–D141.